

Adaptive Asynchronous Control using Meta-learned Neural Ordinary Differential Equations

Achkan Salehi
Sorbonne Université,
achkan.salehi@sorbonne-universite.fr

Steffen Rühl
Magazino GmbH
ruehl@magazino.eu

Stephane Doncieux
Sorbonne Université,
stephane.doncieux@sorbonne-universite.fr

Abstract: Model-based Reinforcement Learning and Control have demonstrated great potential in various sequential decision making problem domains, including in robotics settings. However, real-world robotics systems often present challenges that limit the applicability of those methods. In particular, we note two problems that jointly happen in many industrial systems: 1) Irregular/asynchronous observations and actions and 2) Dramatic changes in environment dynamics from an episode to another (*e.g.* varying payload inertial properties). We propose a general framework that overcomes those difficulties by meta-learning adaptive dynamics models for continuous-time prediction and control. We evaluate the proposed approach on two robotic simulations, the first of which is inspired by a real-world industrial robot.

Keywords: Meta-learning, Neural ODEs, Reinforcement Learning

1 Introduction

Machine Learning methods have increasingly been studied and applied for decision making and control in robotic systems during the past few years. Model-free Reinforcement Learning (RL) methods [1, 2, 3] have shown great success in various robotics tasks, and model-based Reinforcement Learning and Planning [4, 5] have garnered considerable attention due to their increased data-efficiency. More recently, population based methods such as model-free and model-based Quality-Diversity (QD) algorithms [6, 7] have also shown promise in contexts where behavioral diversity is essential.

However, the vast majority of those methods, if not all of them, have been applied in contexts where the difficulties and constraints present in real-world systems are partially relaxed. In particular:

1. In a large number of systems, observations and actions are irregular/asynchronous. This contrasts with the assumptions made by the majority of works in RL/QD, in which actions are applied at a given state and observations are received at regular intervals.
2. The dynamics of the environments in which real-world systems operate are often subject to dramatic discontinuous changes between episodes. This can be for example because of the change in the geometry or mass distribution of a payload, or an unexpected malfunction of some component.

Current work in RL/QD in general only handles one of those aspects, and robust methods for jointly addressing those problems are still lacking. For example, many systems that incorporate meta-learning [8, 2, 9], or system identification [3] are able to adapt to unseen tasks with minimal adaptation. However, to our knowledge, none of these methods address the problem of irregular actions and observations. Similarly, RL methods that are designed to handle those issues and/or operate in continuous-time scenarios [10, 11] are applied to environments that do not change significantly between episodes, and thus do not require much generalization. In contrast, we propose a more general framework that is capable of jointly handling both of the aforementioned problems, and that we have dubbed **ACUMEN**, for Adaptive Control in AsynchronoUs probleM sEttiNgS.

We take inspiration from the industrial robot SOTO, manufactured by Magazino GmbH¹, which manipulates payloads of varying inertial properties. Based on that robot, we develop a simplified, light-weight pybullet [12]

¹<https://www.magazino.eu>

simulation which showcases the advantages of the proposed approach. We also validate our method using the Gazebo Turtlebot3 simulation [13] which relies on ROS² for asynchronous communications with the controller.

The paper is structured as follows. The following section (§2) is dedicated to problem formalization and notations. We position our work with respect to the literature in §3 describe the proposed method in §4. Experimental results are presented in §5. System limitations and future directions are discussed in section §6. Closing remarks are the subject of §7.

2 Problem formulation and Notations

We consider robotic systems with irregular/asynchronous actions and observations that operate in episodic fashion such that the dynamic system governing state transitions is sampled from an unknown distribution for each new episode. We formalize those problems below.

Irregular/asynchronous actions and observations. In most of the RL literature, actions and observations are regular and synchronized: one performs an action a_t in some state z_t , and receives an observation ω_{t+1} . In contrast, we are interested in the general case in which observations and actions are given as $\omega_{t_1}, \dots, \omega_{t_k}$ and $a_{t'_1}, \dots, a_{t'_l}$ with $l \neq k$, $t'_i \neq t_i$. Typically, there might be many actions between two observations, and vice-versa.

We frame such problems as Continuous Time, Partially Observable Markov Decision Processes (CTPOMDP) in which the observation function is time-dependent. More formally, we consider the tuple $\mathcal{T} \triangleq \langle Z, \mathcal{A}, \mathcal{F}, R, \Omega, \Phi, \gamma, T \rangle$ where $Z \subset \mathbb{R}^N$ and $\mathcal{A} \subset \mathbb{R}^M$ respectively denote the state and action spaces. Let us denote $\pi : \mathbb{R} \rightarrow \mathcal{A}$ the function defining the actions to be applied at time t . Then \mathcal{F} defines the evolution of the dynamic system:

$$z(t_0 + \Delta t) = z(t_0) + \int_{t_0}^{t_0 + \Delta t} \mathcal{F}(z(t), t, \pi(t)) dt. \quad (1)$$

The possible time intervals over which the system operates are noted T and the function $\Phi : Z \times T \times \Omega \rightarrow [0, 1]$ defines the probability $p(\omega|z, t)$ of an element ω of the observation space Ω given a state-time pair. In what follows, a_t will denote an action applied at time t . Likewise, ω_t will indicate an observation made at time t . The function $R : Z \times \mathcal{A} \rightarrow \mathbb{R}$ is a dense reward function and $\gamma \in (0, 1]$ is a discount factor. During an episode associated to the tuple \mathcal{T} , our aim is to find $\pi(t)$ that maximizes the discounted cumulative reward $\int_0^\infty \gamma R(z(t), \pi(t)) dt$.

Changes in environment dynamics. We consider the case in which environment dynamics remain stationary through the duration of an episode, but dramatically and discontinuously change in between different episodes. More formally, each task \mathcal{T} is sampled from a distribution of the form

$$P(\mathcal{T}) = P(\langle Z, \mathcal{A}, \mathcal{F}, R, \Omega, \Phi, \gamma, T \rangle) \triangleq P(\mathcal{F}). \quad (2)$$

In other words, two episodes associated to two distinct tasks $\mathcal{T}_i, \mathcal{T}_j$ only differ in \mathcal{F}_i and \mathcal{F}_j , while the rest remains unchanged. An example of this is changes in the geometry and mass distributions of objects being manipulated by a robotic arm. Our objective is to find an adaptive control process $\pi(t, \theta)$ parametrized by θ that leverages previous learning experience to adapt to new, unseen tasks from $P(\mathcal{T})$.

3 Related Work

Model-based Reinforcement Learning and Control. Model-based RL (MBRL) [15] with learned models has been demonstrated to be superior in terms of data-efficiency compared to model-free RL (MFRL), particularly in low-data regimes [16, 17, 4]. This is particularly important on robotic systems, where the large number of interactions required by model-free methods are often impractical. While it has been observed that MBRL can suffer from lower asymptotic performance compared to MFRL [17, 16], recent works [18] demonstrate that this performance gap can be closed by accounting for model uncertainty, which results in better exploration.

A popular approach to Model-based Control is to sample action-state trajectories from the learned model, for example via the Cross Entropy Method (CEM) [19, 5]. Each trajectory is then evaluated based on the predicted states, and the N first actions from the best trajectory are applied on the real system. As a population-based algorithm, the model-based CEM is robust to model inaccuracies, and has been shown to produce results that are on-par with MFRL [18, 20]. Furthermore, CEM, unlike most of the work based on learned policies, is not tied to a particular reward function: indeed, the reward function can be changed at any time during or in-between

²The Robot Operating System[14].

episodes, without any need for additional training. While vanilla CEM suffers from poor data-efficiency in high-dimensional spaces, recent efforts [5] demonstrate that this aspect can be significantly improved, in particular via sampling time-correlated action sequences.

We use CEM-based planning in some of our experiments, and in others, further simplify action selection by sampling from a discrete set of velocity controls. In addition to the reasons that were enumerated above, our choice is motivated by a desire to simplify the decision process, which allows us to focus on the main message of this paper: that combining neural ODEs with meta-learning results in a framework suitable for adaptive control in situations where actions and observations are asynchronous/irregular.

Irregular/asynchronous actions and observations and continuous time control. The vast majority of the RL literature considers discretized time-steps with regular observations and actions, and most prior work on continuous time systems make simplifying assumptions such as partially known and/or linearized dynamics systems [21, 22, 23], or are applied in model-free settings [24, 25]. However, more recent efforts build on Neural Ordinary Differential Equations (N-ODEs) which outperform discrete approaches to modeling continuous-time dynamics [26]. In their work, Du et al. [11] model environment dynamics using N-ODEs in order to learn policies in semi-MDP problem settings, while the continuous-time RL framework of Yildiz et al. [10] is notable for providing state uncertainty estimates. While our use of N-ODEs is similar to what was done in those works, it should be noted that our focus is on an orthogonal direction: our aim is to investigate the combination of meta-learning and N-ODEs in order to simultaneously address the problem of irregular/asynchronous actions and observations and discontinuous changes in system dynamics on a per episode basis. This distinction is reflected in our experimental setup, which is closer to real-world applications.

Meta-learning. Leveraging previous experience to improve the learning process has been extensively studied in the meta-learning [27, 28] literature. As even when considering the most restrictive definitions of meta-learning in which identical train/test conditions, end-to-end optimization and sample splitting are essential [27], one is left with a plethora of methods that differ, among other things, in what meta-parameters they optimize. For example, many meta algorithms learn a recurrent network that models policies [29] or optimizers/update rules [30], while others optimize hyperparameters [31] or metrics [32]. It is thus important to note that the meta-parameter that we seek to optimize is a prior dynamics model (more precisely, a neural ODE), which when used as an initialization in novel control tasks, should be able to quickly adapt to represent the dynamics of that environment. Learning adaptive priors is precisely what algorithms in the MAML family [8, 33] are designed for. In particular, we update our parameters in a manner similar to ES-MAML [33], as it alleviates the need for the estimation of second order neural ODE derivatives.

4 ACUMEN

We propose an algorithm based on Model Predictive Control (MPC) [5, 15] with a learned and dynamically adapted environment model based on the formalism of Neural Ordinary Differential Equations (N-ODE) [26]. In order to ensure performance on unseen tasks, learning experience from previous episodes is used to maintain a prior on the weights of the N-ODE with which each new episode is initialized. Each of the following subsections is dedicated to one of those components. An overview of our approach is given in algorithm 1.

4.1 Handling irregular/asynchronous observations and actions

As the state in the problem settings that we discussed in section §2 is partially observable, we assume the existence of a learned or hand-designed function $\xi_n : \omega_0 \times \omega_1 \times \dots \times \omega_n \rightarrow Z$ that maps a sliding window of observations $W = \{\omega\}_{i=1}^n$ to a state approximation, i.e. $\xi(W) = \hat{z} \in Z$. When clear from context, we will drop the window size from the notation and simply write ξ . We then use a neural ODE $\hat{\mathcal{F}}$, parametrized by weights θ to approximate the dynamics evolution function \mathcal{F} :

$$\hat{z}(t_0 + \Delta t) \approx \hat{z}(t_0) + \int_{t_0}^{t_0 + \Delta t} \hat{\mathcal{F}}(\hat{z}(t), t, \pi(t), \theta) dt. \quad (3)$$

As we are interested in irregular actions, the function π will in effect be the composition of two functions: a decision process $u(t_0 - s, t_0 + \Delta t)$ that outputs irregular actions at discrete timestamp falling in $[t_0 - s, t_0 + \Delta t]$, and an interpolation function that interpolates those actions to produce action values at continuous timestamps. More formally, π can be written as

$$\pi(t) = (\mathcal{I} \circ u(t_0 - s, t_0 + \Delta t))(t) \quad \forall t \in [t_0 - s, t_0 + \Delta t] \quad (4)$$

for some (small) real value s . In our work, the interpolation \mathcal{I} is the linear interpolation function.

Algorithm 1: The ACUMEN algorithm.

Input: Task distribution $\mathcal{P}(\tau)$, number of tasks to sample for each meta update N , train/validation split ratio $r_{split} \in (0, 1)$, maximum number of iterations for inner loop (neural ODE) optimizations N_{it} , optionally prior parameters of the N-ODE θ_0 , hyperparameters `action_selection_hyperparams` (see algorithm 2), function ξ mapping sliding windows of observations to state approximations, size of sliding window of observations M , learning rate for the meta update α , standard deviation σ for the estimation of the meta update

Output: prior parameters to use for future sessions θ

```
1
2  $\theta \leftarrow \text{RandomInit}()$  if  $\theta_0$  is not given; else  $\theta \leftarrow \theta_0$ 
3 while session no over do
4   // sample i.i.d vectors for the ES update of the meta-parameters
5    $\epsilon_1, \dots, \epsilon_N \sim \mathcal{N}(\mathbf{0}, \mathbf{I})$ 
6   for  $i \in \{1, \dots, N\}$  do
7      $\tau_i \sim \mathcal{P}(\tau)$ 
8      $\mathcal{D}_i^{train} \leftarrow \emptyset$ 
9      $\mathcal{D}_i^{val} \leftarrow \emptyset$ 
10     $\theta_i^* \leftarrow \theta + \epsilon_i \sigma$ 
11     $C_{hist} \leftarrow \emptyset$  // history of applied actions
12    while not ( $\tau_i.success$  or  $\tau_i.timeout$ ) do
13      // get the  $M$  most recent observations
14       $\omega_1, \dots, \omega_M = \tau_i.get\_sliding\_window(M)$ 
15      // get all actions sent since the oldest observation in the window
16       $c_1, \dots, c_l = \text{GetAllActionsSince}(\omega_1.timestamp, C_{hist})$ 
17      // Map the sliding window to a state approximation
18       $\hat{z} = \xi(\omega_1, \dots, \omega_M)$ 
19      // Choose the next action sequence (see algorithm 2 for details)
20       $seq = \text{SelectNewCommand}(\theta_i^*, \hat{z}, \{c_1, \dots, c_l\}, \text{action\_selection\_hyperparams})$ 
21      // Apply the  $K$  first actions in the sequence
22       $\tau_i.Apply(seq_{1:K})$ 
23      // Add the applied actions to command history
24       $C_{hist}.append(seq_{1:K})$ 
25      // split gathered data into train/validation sets
26       $d_{train}, d_{val} \leftarrow \text{sample\_split}([\omega_1, \dots, \omega_M], [c_1, \dots, c_l], r_{split})$ 
27       $\mathcal{D}_i^{train}.append(d_{train})$ 
28       $\mathcal{D}_i^{val}.append(d_{val})$ 
29      // optimize the prior if necessary (see appendix A for details on OptimizeNODE)
30      if train_freq then
31        |  $\theta_i^* \leftarrow \text{OptimizeNODE}(\theta_i^*, \mathcal{D}_i^{train}, N_{it})$ 
32      end
33    end
34  end
35  // update the meta-parameters  $\theta$ 
36   $\theta \leftarrow \theta - \frac{\alpha}{N\sigma} \sum_{i=1}^N \mathcal{L}_i(\theta_i^*, \mathcal{D}_i^{val}) \epsilon_i$ 
37 end
```

Algorithm 2: An action selection step using the learned neural ODE. While predicted actions $a_{1:H}^i$ are regularly sampled, their application on the system will be irregular. Thus, the history of actions c_1, \dots, c_n will be composed of irregularly applied actions, hence the advantage of using the neural-ODE formalism. Note that while the action sampling process outlined here includes CEM-based sampling with time-correlated actions (as in [5]) as a special case, it can also be reduced to a simple random shooting depending on the choice of $P_\psi(A)$ and other hyperparameters. We will adjust those on a per application basis in our experiments. See sections 5 and appendix B for more details.

Input: Neural ODE weights θ , state approximation $\hat{z}(t_0)$ at time t_0 , desired duration of state propagation Δt , previous actions c_1, \dots, c_l (augmented with their timestamp info), number of action sequences N_p to sample, number of elite action sequences N_e , length of action sequence to sample H , reward function $R(\cdot)$, prior distribution on actions $P_\psi(A)$ (parametrized by ψ), initial parameters ψ_0 for $P_\psi(A)$, convergence criterion \mathcal{Y}

Output: action sequence a_1^*, \dots, a_H^*

```

1 Function SelectNewCommand( $\theta, \hat{z}(t_0), \Delta t, \{c_1, \dots, c_l\}, N_p, H, R(\cdot), \mathcal{Y}$ ):
2    $\psi = \psi_0$ 
3   // initialize elite set
4    $\mathcal{E} = \emptyset$ 
5   while not  $\mathcal{Y}$  do
6     // sample  $N_p$  action sequences of length  $H$  at regular intervals in  $[t_0, t_0 + \Delta t]$ 
7      $a_{1:H}^1, \dots, a_{1:H}^{N_p} \sim P_\psi(A)$ 
8     for each  $a_{1:H}^i$  do
9        $u_i = [c_1, \dots, c_l].\text{concatenate}(a_{1:H}^i)$ 
10      // Let  $\pi_i(t)$  the function that computes actions via interpolating elements of  $u_i$ 
11       $\pi_i = \mathcal{I} \circ u_i$ 
12      // propagate the state
13       $\hat{z}_i = \hat{z}(t_0) + \int_{t_0}^{t_0 + \Delta t} \hat{\mathcal{F}}(\hat{z}(t), \pi_i(t), \theta) dt.$ 
14      // compute associated reward
15       $r_i = R(\hat{z}_i)$ 
16    end
17     $\mathcal{E} = \text{select best } N_e \text{ action sequences according to the } r_i$ 
18    // Update prior distribution  $P_\psi(A)$  on commands
19     $\psi \leftarrow \text{updatePriorDistribution}(a_{1:H}^1, \dots, a_{1:H}^{N_p}, r_1, \dots, r_{N_p})$ 
20  end
21  // return the best action sequence (alternatively, re-sample from  $P_\psi(A)$ )
22  return  $\mathcal{E}$ 

```

In our action-sampling based system (algorithm 2), N_p different action sequences, each of length H , are sampled and considered as possible continuations of the current history of actions. Each of these action sequences can be thought of as a decision process u_i (with $i \in \{1, \dots, N_p\}$). Since the interpolation function \mathcal{I} is fixed, it is equivalent to say that we samples N_p functions $\pi_i \triangleq \mathcal{I} \circ u_i$.

4.2 Planning with a continuously updated model

The proposed method is based on Model Predictive Control (MPC) with a learned model, that is updated throughout the duration of an episode. At each iteration of the algorithm (lines 11-28 in algorithm 1), a sliding window consisting of the last M observations $\{\omega_1, \dots, \omega_M\}$ is mapped to a state estimation $\hat{z}(t)$. Actions $\{c_1, \dots, c_l\}$ (in general, $l \neq M$) that have been applied since the time at which ω_1 was observed are gathered. All observations and actions are added to a buffer with the aim of updating the model.

We determine an action sequence $a_{1:H}^*$, that when appended to $\{c_1, \dots, c_l\}$, would result in the most promising future state according to the predictions of the learned model. The sampling and selection process is detailed in algorithm 2. As previously discussed in detail in section §3, our decision to rely on command sampling is not only motivated by its demonstrated efficacy and robustness, but also by its simplicity.

Once a sequence $a_{1:H}^*$ has been selected, its first action is applied on the system. The learned model is updated every *train_freq* iterations.

4.3 Learning a neural ODE prior

Our objective of obtaining a point-wise estimate of weights that could serve as an adaptive prior in environments with previously unseen dynamics can be formulated via the following equation:

$$\theta \leftarrow \theta - \alpha \nabla \sum_{i=1}^N \mathcal{L}(\mathcal{T}_{val}^i, \theta - \lambda \nabla \mathcal{L}(\mathcal{T}_{train}^i, \theta)) \quad (5)$$

in which $\mathcal{L}(\cdot, \theta)$ denotes the training loss of a neural ODE on some dataset. As is classically done in the meta-learning literature for the sake of conciseness in notations, each of the inner and outer optimization problems have been written as a single gradient descent update. However, in practice the number of updates is arbitrary.

Notice that the inner optimizations, *i.e.* $\theta - \lambda \nabla \mathcal{L}(\mathcal{T}_{train}^i, \theta)$, correspond to model-predictive episodes (lines 11-28 in algorithm 1).

Computing the gradient update for the outer level optimization problem requires differentiating through the gradient computed in the inner optimization. As this would necessitate computing higher order derivatives of neural ODEs, we simplify the outer level update by using an estimator based on Evolution Strategies [34]:

$$\frac{1}{\sigma} \mathbb{E}_{\tau \sim P(\tau), \epsilon \sim \mathcal{N}(0, I)} [\mathcal{L}(\mathcal{T}_{val}^\tau, \theta + \epsilon - \lambda \nabla \mathcal{L}(\mathcal{T}_{train}^\tau, \theta + \epsilon)) \epsilon]. \quad (6)$$

Note that this update, approximated using N sampled environments in algorithm 1 (line 30) is equivalent to the zero-order ES-MAML update [33].

5 Experimental Validation

We present experiments on two simulated robots. The first one is inspired by the SOTO robot manufactured by Magazino GmbH, and uses two conveyor belts to manipulate boxes of different inertial properties. As the simulation is developed in pybullet [12], command and observation irregularities are simulated by randomly dropping observations and by applying interpolated commands at random timestamps. The second experiment is based on the Gazebo Turtlebot3 simulation[13]. As communicating with the Gazebo simulator is done via ROS topics and services, the observations and actions already suffer from some irregularity that we further accentuate by dropping random observations in order to better highlight the advantages of using neural ODEs. For both robots, the physical properties of the environment are randomly sampled at the beginning of an episode.

In addition to evaluating the ability of the ACUMEN algorithm to jointly address asynchronous/irregular actions and observations as well as discontinuous changes in environment dynamics, we also highlight the effect of its different components through ablation studies. In particular, we highlight the advantages of using neural-ODEs. Classical model-based RL approaches usually learn a model of the form $\Delta z_{t+1} = M(z_t, a_t)$, which corresponds to (PO)MDPs. A simple extension to that model for the case of irregular/asynchronous actions can be obtained by considering a recurrent neural network which would take as input the sequence of tuples $(a_0, \Delta t_0), \dots, (a_n, \Delta t_n)$ with Δt_i the elapsed time between a_i and a_{i+1} for $i \neq n$, and Δt_n the elapsed time between a_n and the next observation (or during planning, the next predicted state). In this paper, we implement this model as a vanilla stacked RNN. Note that this is a slight generalization of state propagation of the form $z_t = z_{t-1} + M(z_{t-1}, a_{t-1}, \Delta t_{t-1})$ which was shown in prior work [10] to be inferior to neural ODEs in continuous time settings. In the rest of the paper, we will use the terms RNN and stacked RNN and recurrent model interchangeably when the context allows it.

Details regarding loss and reward functions as well as various hyper-parameters can be found in the appendixes.

5.1 Simulated box rotation using conveyor belts

This robotic simulation is inspired by the SOTO robot manufactured by Magazino GmbH. Before presenting our results, we detail the simulation as well as some algorithmic choices in the following section. Results from the complete system are presented in section 5.1.2, and ablation studies follow in sections 5.1.3.

5.1.1 Simulated Box rotation: experiment description

The simulation, developed using the bullet physics engine [12], defines the following problem: given two parallel and independently controlled conveyor belts separated by some distance (figure 1(a)), the aim is to rotate a parcel by $\frac{\pi}{2}$ radians. The default problem setting is illustrated in figure 1(c). At the beginning of an episode, a box of varying inertial properties is sampled from a distribution $P(\mathcal{T}_{box})$, and is positioned (plus or minus some gaussian noise) at the pose shown in figure 1(c, left). The task is considered solved if the system

reached (with some tolerance) the state given in the right hand of figure 1(c). The environment, shown in 1(b), is based on simulated roller conveyors [35].

The box distribution $P(\mathcal{T}_{box})$ is defined by a random choice of mass in the interval $[0.1kg, 3kg]$ and a mass distribution given by random $3d$ Gaussian distributions, which can have dense covariances. To simplify matters, we use ground truth $6d$ box poses as observations. Given the last two observed box poses ω_{t-1}, ω_t , we approximate the state to propagate as $\hat{z} = [\omega_t, \frac{\omega_t - \omega_{t-1}}{\Delta t}]$. Note that the action space is two-dimensional and defined by $[-1, 1] \times [-1, 1]$, as each of the conveyors can receive velocity controls independently of the other one. The distance from a given pose and the target pose is used as a dense reward signal to guide the action selection process. The action sampling mechanism that is used is a particular instantiation of algorithm 2 which is equivalent to the CEM-based control method with colored noise from [5]. Details are given in appendix B.

For benchmarking purposes, we define each timestep as the time elapsed between applying actions in the physics engine, which is done at regular intervals. We however emphasize that those actions are not used by our control algorithm, which only receives actions that the result of linear interpolations at random time-steps. The maximum number of timesteps for each episode is set to $H_{max} = 300$.

In all experiments, the RK45 solver [36] (commonly referred to as `dopri5`) is used.

Irregular/asynchronous observations and actions. We simulate irregular/asynchronous observations and actions by 1- Returning only one random observation among K_s successive observations, 2- returning actions at randomly interpolated time-stamps in between real actions and 3) Discarding selected observations with some probability η . In the following experiments, a value of $K_s = 3$ has been chosen, and $\eta = 0.05$. The colored noise parameter used in CEM-based sampling (algorithm 3) was set to $\beta = 2$.

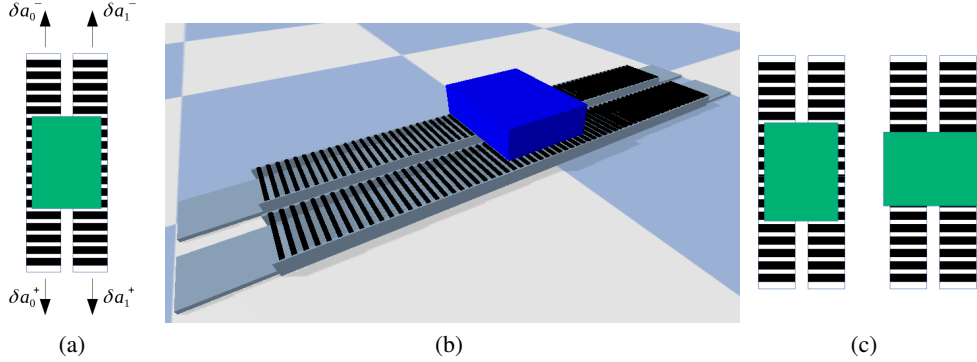


Figure 1: **(a)** Schematic view of the system, showing a green box on top of two conveyor belts. The conveyor belts are independent, and the motion of each one is controlled via a one-dimensional velocity command in $[-1, 1]$. Positive and negative actions, *e.g.* $\delta a_0^+, \delta a_0^-$ respectively move the left conveyor in the top or bottom direction. Commands such as $\delta a_1^+, \delta a_1^-$ should affect the right-hand conveyor belt in similar fashion. **(b)** Screenshot of the developed robot simulation, based on simulating two roller conveyors. **(c, left)** Illustration of the initial conditions in each episode. **(c, right)** Target pose that we aim to reach through controlling the conveyor belts. Note that the mass and inertial properties significantly and discontinuously vary in-between episodes.

5.1.2 Simulated box rotation: system results

The objective of this subsection is to validate the complete system in the presented simulation, where irregular/asynchronous actions and observations have been simulated, and where environment dynamics vary from one episode to the next due to the random sampling of box mass and inertial properties.

A neural ODE is initialized with random weights, and receives successive meta updates in order to form the learned prior. In each meta iteration, $N = 20$ tasks τ_1, \dots, τ_N are sampled from the environment distribution. As detailed in algorithm 1, the neural ODE is independently adapted to each of the τ_i using data gathered during the episode, the validation split of which is then used in the meta update.

The result of the experiment are plotted in figure 2. As figure 2(a) shows, at initialization, model-predictive control with the random neural ODE is only able to solve about 5% of the environments that are sampled from the test distribution. In this first meta iteration, the variance of episode lengths (figure 2(b)) is large, with most episode requiring many updates to the neural ODE. Hence, the large mean episode length reported in that same figure.

It can be seen that as the learned prior is optimized during successive meta-iteration, the percentage of successfully solved test environments increases until eventually reaching a point where it oscillates between 95–100%

(figure 2(a)). Simultaneously, the number of steps spent across all environments (solved and unsolved) decreases as the optimization of the prior progresses (figure 2(b)).

Figure 2(c) shows the number of timesteps spent in environments that the system was able to solve at a given meta iteration. After an initial large drop in mean and variance in the first few (< 10) meta iterations, the number of necessary steps for solving an environment stabilizes to around 100 timesteps, while the number of success (figure 2(a)) continues to grow. A possible explanation for this phenomenon comes from observing the behavior of models specialized for an environment, an example of which will be discussed in the next subsection. Models that are specialized to an environment result in near-optimal state-action trajectories connecting the initial box pose to the target pose, and take about 40 to 50 timesteps. A general prior would then be positioned in some area of parameter space minimizing its average distance to several specialist networks, hence the higher number of updates necessary for its adaptation.

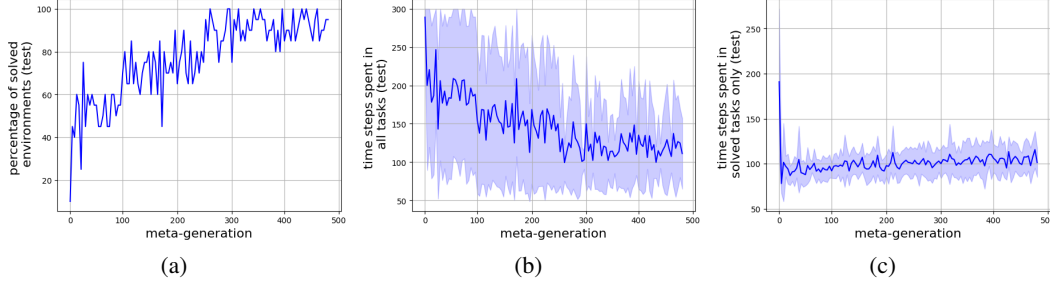


Figure 2: **(a)** The evolution of the percentage of solved environments among the $M_{test} = 20$ ones that are sampled from the test distribution $P(\mathcal{T}_{box})$ at each meta-generation, starting from a random neural ODE. **(b)** In this figure, the value displayed at each meta-generation is the time spent in all tasks (solved and unsolved) that have been sampled at this meta-iteration. **(c)** Same as in **(b)**, but for solved environments only. Notice the large drop in the number of necessary timesteps in the ~ 10 first meta-generations.

5.1.3 Simulated box rotation: Ablations

Our principal aim in this paper is to investigate the advantages of combining meta-learning and neural-ODEs in the contexts that were previously discussed. Therefore, we consider two ablation experiments. In the first one, we consider two different manners in which the meta-update component can be removed. In the second ablation study, we compare a specialized neural ODE to a specialized Recurrent network.

Meta-update ablation. We first naively disable the meta-update in ACUMEN. The results of this experiment are reported in figure 3. Unsurprisingly, without the meta update, the adaptations that the neural ODE goes through within distinct episodes is only sufficient for solving on average about $\sim 9\%$ of the sampled tasks in the given time limit of $H_{max} = 300$ (which is the same as in all our simulation-based experiments). The number of timesteps solved in all environments (solved or unsolved) displays significantly higher mean and variance.

To further investigate the advantages of the learned prior, we compare its performance with that of a specialist model trained until convergence on a single "average" environment, henceforth noted E_1 , given by a box with mass $1.5kg$ and uniform mass distribution. The results are compiled in table 1. As expected, the learned prior is able to adapt to and solve 91.3% of the environments within the (per episode) time limit of H_{max} , while the specialized model is able to solve 77.8% of the environments. The number of timesteps spent across all environments has lower mean and standard deviation $\mu_{time}, \sigma_{time}$ when the learned prior is used. It is however interesting to note that the specialized model can more easily solve environments that are close to the task it has been trained for. This is why \min_{time} , the minimum number of necessary timesteps across all environments is lower for the specialized environment in table 1.

	#sampled environments	success	μ_{time}	σ_{time}	\min_{time}
learned general prior	600	548 (91.3%)	121.943	57.85	58
specialized model	600	467 (77.8%)	127.513	92.26	40

Table 1: Comparison between the prior learned by ACUMEN and a specialized model trained in an average environment on 600 randomly sampled boxes. Here, $\mu_{time}, \sigma_{time}$ denote the mean and average of the number of timesteps spent in a given environment, which are both lower for the learned prior. The minimum number of time-steps used to solve an environment is denoted \min_{time} .

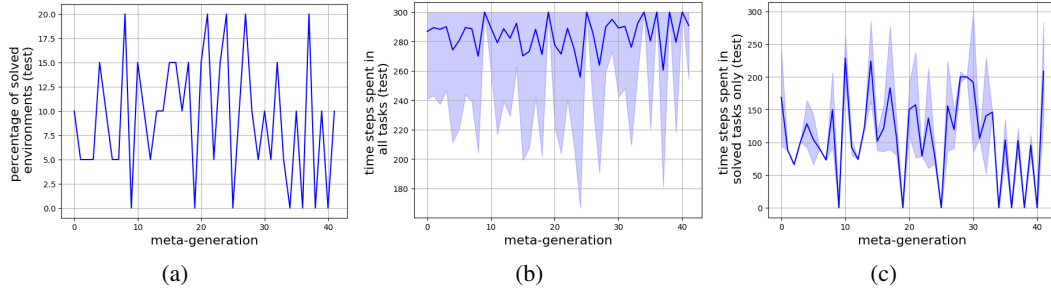


Figure 3: Result of meta-update ablation. **(a)**. It can be seen that a random neural ODE can be adapted to solve an average of 9% of the sampled environments in the given time limit of $H_{max} = 300$. **(b)** Naturally, without the meta-update, there is no reduction in the average time taken to solve the environments. **(c)** The average and the variance of time-steps spent across solved environments only. Values of zero indicate that none of the environments were solved. The remaining values are in general larger than those that were reached at convergence with the meta-update enabled (figure 2(c)).

	Neural ODE	RNN
#episodes	30	30
success	24 (80%)	15 (50%)
μ_{time}	58.125	109.26
σ_{time}	10.89	34.93
med_{time}	59.15	107.0

Table 2: Comparison between a specialized neural ODE and a specialized RNN.

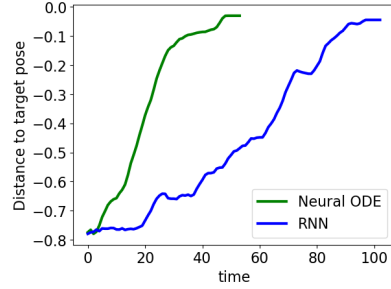


Figure 4: Comparison between typical trajectories resulting from neural ODEs vs RNNs.

Neural-ODE ablation. As discussed in the beginning of section 5, we compare the results obtained with a neural ODE with those obtained with a stacked RNN, which takes as input the sequence of tuples $(a_0, \Delta t_0), \dots, (a_n, \Delta t_n)$ with Δt_i the elapsed time between a_i and a_{i+1} for $i \neq n$, and Δt_n the elapsed time between a_n and the next observation (or during planning, the next predicted state).

For this experiment, we considered an environment with fixed dynamics, that we will note E_2 , corresponding to a mass of $0.5kg$ and uniform mass distribution. The stacked RNN was first pretrained on data from that environment, which were gathered from three episodes with significant action-state coverage: one with random controls, one successful episode with neural-ODE based control, and another episode using the same neural-ODE but with noise injected into the actions. It was then compared during 30 model-predictive trials to the specialist neural-ODE model that was learned in the previous section on the E_1 environment. Note that while the dynamic system is fixed, the observations and actions change from one episode to the other, as they are the result of interpolations at random timestamps, as previously specified in section §5.1.1. The results are reported in table 2.

It can be seen that the ODE-based network, specialized for the E_1 environment, performs significantly better than the recurrent model on the E_2 model, for which the latter is a specialist. This is expected, as the recurrent model is equivalent to linearizing the dynamics model on a much coarser scale than what an ODE solver would do. Figure 4 shows two example box pose trajectories from successful episodes, one obtained using the neural ODE (in green), and the other from using the recurrent model (blue curve). Each curve represents the distance from the current pose to the target state. It can be seen that the trajectory obtained with the neural ODE is much smoother than the one resulting from the stacked RNN.

5.2 Gazebo Turtlebot3 simulation

We describe the simulation and tasks in section §5.2.1. In section §5.2.2, we define different levels of irregularity in the data, and compare the use of neural ODEs and RNNs for controlling the turtlebot in each of those

settings. The complete system’s ability to adapt to unseen environment physical properties is then evaluated in section §5.2.3.

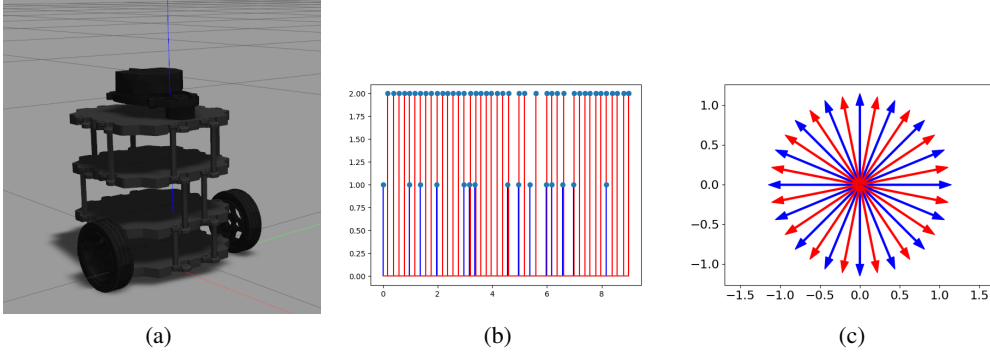


Figure 5: (a) The turtlebot simulation (b) Stem-plot showing an example of observation (in blue) and action (in red) occurrence. In this particular example, observations are dropped with probability $P_{drop} = 0.5$, further accentuating the asynchronous/irregular nature of actions and observations. (c) The wind directions used to define the task distributions. blue arrows indicate directions that are used for training and meta-updates, and red arrows show the directions on which the test distribution is based.

5.2.1 Gazebo turtlebot3 simulation: description

This simulation [13] uses the ROS Gazebo [37] package and is therefore closer to a real robotic system than the pybullet simulation discussed in the previous section. Furthermore, policies trained in this simulation or more generally with Gazebo simulation can be successfully transferred to real systems, although strategies such as domain randomization are often necessary to avoid overfitting to the simulator [38, 39, 40]. A screenshot of the simulation is given in figure 5 (a).

The command space of the robot is given by $[-0.22, 0.22] \times [-0.22, 0.22]$ for linear and angular velocity control³. We use the pose estimation of the robot—as published to the /odom topic by the Gazebo turtlebot3 simulation—as the observation, but reduce the publication frequency of that information to $\sim 6hz$. As in the box rotation experiments, we approximate the state to propagate as $\hat{z} = [\omega_t, \frac{\omega_t - \omega_{t-1}}{\Delta t}]$ where ω_{t-1}, ω_t are the two last pose observations.

In all experiments, the robot starts at the origin and its objective is to navigate to an arbitrarily set target. We will first compare the effectiveness of RNNs and neural ODEs when faced with different levels of irregularity, that will be defined by the probability P_{drop} of dropping observations. Note that even $P_{drop} = 0$ will result in irregularity in the data as a result of the asynchronous nature of ROS. An example of action and observation occurrences during a randomly selected time interval with value $P_{drop} = 0.5$ is shown in figure 5.

The comparisons between neural ODEs and recurrent models which are presented in sections 5.2.2 use the default settings of the simulator, where except for gravity, no external forces are applied to the robot. In order to evaluate the ability of the complete system to adapt to unseen environment physics (section §5.2.3), we additionally define a distribution over physical properties of the simulation which are given by a choice of constant “wind” that is implemented as a constant acceleration applied to the robot. For simplicity, we consider a discrete set of directions, uniformly spaced on the unit circle (figure 5(c)), and a discrete set of magnitudes. Details on the different splits used for training, meta-updates and tests will be given in section §5.2.3.

Note that the particular instance of algorithm 2 which is used in this section is equivalent to a simple random shooting (appendix B). While this sacrifices some precision, it allows the algorithm to publish decisions at a higher rate. The same motivation led us to replace the adaptive-step solver of the previous experiments by a fixed step ODE solver (RK4) which proved sufficient for controlling the turtlebot.

5.2.2 Gazebo turtlebot3 simulation: neural ODEs vs stacked RNNs

Here we concentrate on control using an environment with fixed physical properties in order to investigate the advantages of neural ODEs for control in the case of irregular/asynchronous observations. The physical properties are set to the defaults and no wind is applied. As in the previous section, we use a stacked RNN—the hyperparameters of which are specified in appendix D—as a baseline. Note that both the RNN and the N-ODE are pre-trained until convergence with $P_{drop} = 0$ and using continuous actions that are sampled according to a

³The maximum absolute value of the angular velocity that can be sent to the turtlebot is 2.84, but we use a lower value in order to simplify the dynamics.

uniform distribution over $[-0.22, 0.22]$ for both the linear and angular velocity controls. However, as detailed in appendix B, during control, actions are selected among a discretized set of velocity controls.

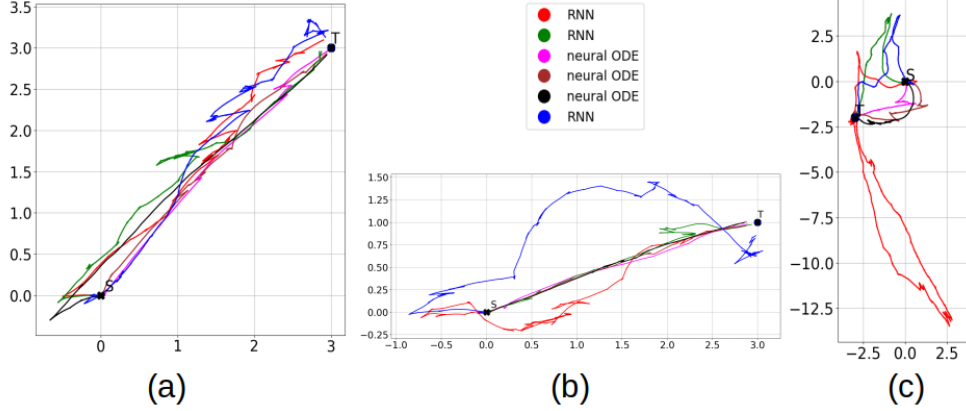


Figure 6: Examples of trajectories obtained with Neural ODEs and RNNs for different values of P_{drop} . In all figures, the initial position of the robot and the target pose are respectively noted S, T . **(a)** Trajectories obtained when $P_{drop} = 0$. Note that in this case, irregularities in the input data are still present due to the asynchronous nature of ROS. **(b)** Example trajectories with $P_{drop} = 0.2$. **(c)** Trajectories obtained with $P_{drop} = 0.5$.

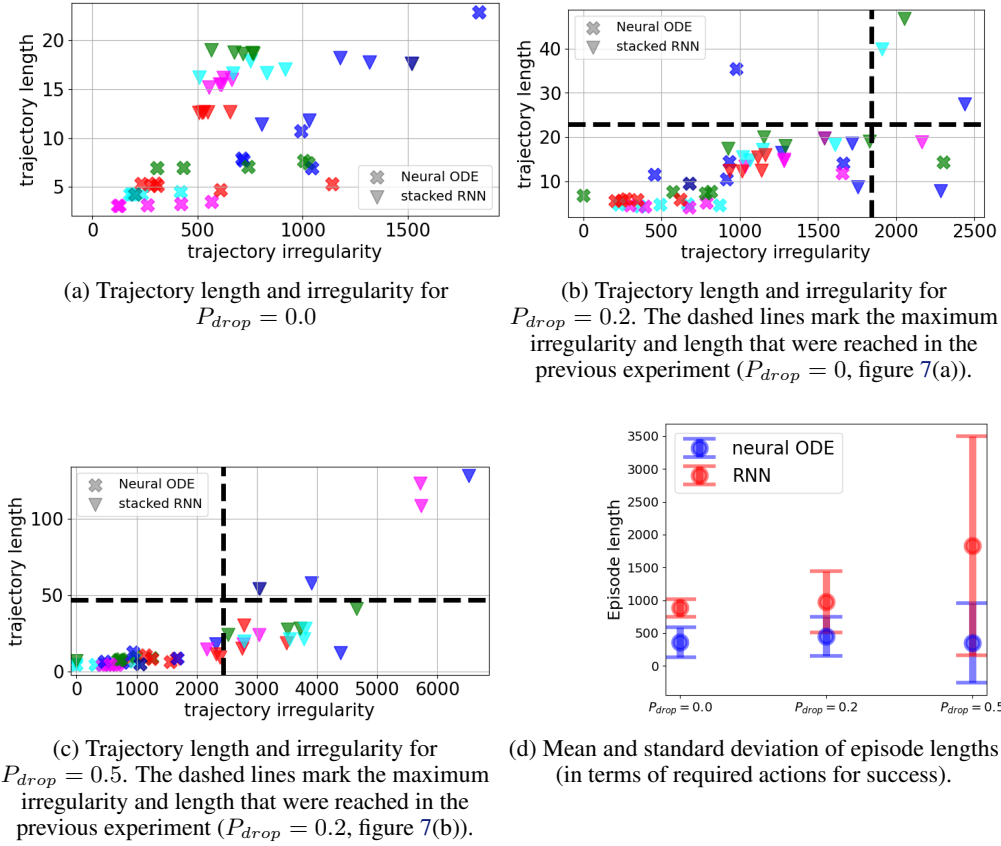


Figure 7: **(a)**, **(b)**, **(c)** each correspond to 50 experiments corresponding to a value of P_{drop} , such that half experiments use a neural ODEs and the other half uses a recurrent model. The experiments in which the positional target of the robot was the same are indicated using the same color. **(d)** compares the length of episodes in terms of number of commands necessary to reach the goal.

In many real world robotic systems ⁴, different components often publish asynchronously to different topics and at different frequencies based on multiple hardware and software related constraints. This can result in significant irregularities. As controlling the simulated turtlebot is done via those same publication, subscription and service mechanisms, irregularities in actions and observations also naturally occur. However, in these simplified settings, those irregularities are rather small. Therefore, we introduce an additional source of irregularity by dropping each in-coming observation with a probability of P_{drop} . In what follows, we compare the RNN and the N-ODE for values of $P_{drop} = 0, 0.2, 0.5$. Figure 5(c) shows a stemplot of command/observation occurrences for $P_{drop} = 0.5$.

Figure 6 shows a few example trajectories for different values of P_{drop} and arbitrary set target positions. It can be seen that the performance of the RNN drops significantly as P_{drop} increases, while the impact on the neural ODE is limited. Indeed, while the trajectories obtained with the neural ODE remain short and smooth for different P_{drop} values, the trajectories produced when using the stacked RNN become longer and less regular with the increase of P_{drop} .

Quantitative results. We ran a total of 150 control experiments, in which the initial position of the robot was set to the origin and its orientation to the identity matrix. Each experiment was fully determined by the choice of

1. a pretrained model: RNN or neural ODE,
2. a target out of five possible positions⁵.
3. Observation drop probability P_{drop} , chosen in the set $\{0.0, 0.2, 0.5\}$.

resulting in 30 possible combinations, and ran each of them 5 times. The trajectories were compared according to three characteristics:

1. Trajectory length. This is just the length of the curve.
2. Irregularity, which we define as $S_\kappa \triangleq \int_a^b \kappa(s) ds$, where κ is the unsigned curvature and ds is the length element.
3. Episode length in terms of number of applied actions.

Indeed, while shorter and smoother trajectories are desirable, a control process that would only chose conservative, small actions might indicate poor predictions from the learned model, hence the consideration of the number of actions as the third characteristic.

The results are reported figure 7. Note that in figures 7(a, b, c), markers of the same color correspond to episodes that had the same positional target for the robot. As it can be seen in figure 7(a), the small irregularities that are present due to the asynchronous nature of ROS in general seem to result in trajectory lengths and irregularities that are slightly larger for the recurrent models. As we increase P_{drop} to 0.2 (figure 7(b)), the trajectories become longer and less regular for both models. However, the effect is more pronounced for the RNNs, in particular in terms of trajectory irregularity: neural ODEs mostly remain in the same interval ($S_\kappa < 1000$) as in the previous experiment ($P_{drop} = 0$, figure 7(a)), but the majority of RNNs produce trajectories with irregularities $S_\kappa > 1000$ while that was not the case in the previous experiment with $P_{drop} = 0$. As for trajectory lengths, RNNs more frequently produce trajectories with lengths greater than the upper bounds on the results of the previous experiment (dashed lines in figure 7(b)).

The gap between the performances of neural ODEs and RNNs is widened further as P_{drop} is increased to 0.5 (figure 7(c)). The majority of lengths and irregularities of the trajectories generated by RNNs takes values greater than the upper bounds on previous experiments (dashed line in figure 7(c)). The lengths in particular are increased by factors of up to 5, while irregularities are increased by factors of up to 3. On the other hand, length-wise, the trajectories generated by neural ODEs remain in the same interval as in the previous experiments. The increase in irregularity is also much less pronounced than with the recurrent models.

Neural ODEs also outperform the considered RNNs in terms of number of required actions. As shown in figure 7(d), the average number of actions necessary for success using neural ODEs is upper bounded by the corresponding value for RNNs which significantly increases with P_{drop} .

⁴We exclude real-time Operating Systems from this discussion.

⁵The target position were set over all quadrants of the xy plane in an arbitrarily manner to $\{(3.0, -2.0, 0.0), (-3.0, -2.0, 0.0), (3.0, 1.0, 0.0), (3.0, 3.0, 0.0), (2.5, 6.3, 0.0)\}$

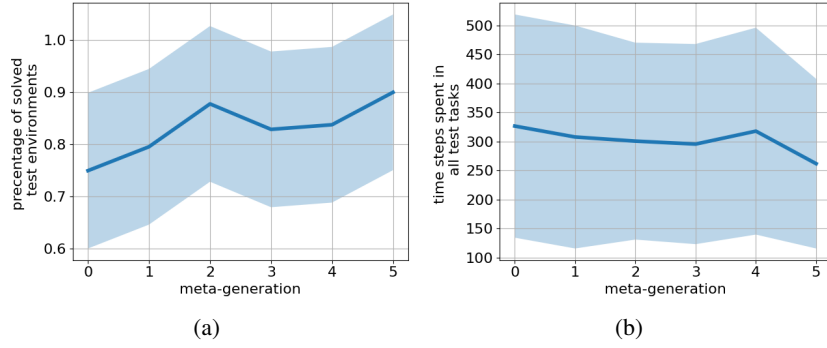


Figure 8: The effect of a few meta-updates to the pretrained neural ODE, averaged over three distinct execution. Both figures show average values and one single standard deviation.

5.2.3 Gazebo turtlebot3 simulation: Adaptation to novel dynamics

As mentioned in section §5.2.1, a distribution of physical properties based on applying “wind” as a constant acceleration vector defines the task distribution $P(\mathcal{T}_{turtle})$ that we consider. More formally, noting $S_{mag} \triangleq \{0.1, 0.2, 0.4, 0.5\}$ the set of possible magnitudes, the train and test task distributions are given by

$$\begin{aligned}
 P(\mathcal{T}_{turtle})^{train} &\triangleq \mathcal{U}(\{[\cos(u), \sin(u)]^T | u = n \frac{2\pi}{n_d} \quad \forall n = 2k, k \in \mathbb{Z}\} \times S_{mag}) \\
 P(\mathcal{T}_{turtle})^{test} &\triangleq \mathcal{U}(\{[\cos(u), \sin(u)]^T | u = n \frac{2\pi}{n_d} \quad \forall n = 2k + 1, k \in \mathbb{Z}\} \times S_{mag})
 \end{aligned} \tag{7}$$

where \mathcal{U} denotes the uniform distribution and n_d is the number of wind directions. In our implementation, we chose $n_d = 32$, resulting in 16 directions for each of the train and test splits (figure 5(c)).

Setting $P_{drop} = 0.5$ and starting with the pretrained neural ODE of section 5.2.2, we evaluated the effect of meta-updates, each based on $N = 25$ train tasks. As the asynchronous nature of the publishing/subscription/service mechanisms can lead to different outcomes on each execution, we averaged the results of three distinct experiments, each making 5 updates to the initial model. The results, displayed in figure 8 (a,b), indicate that just a few iterations result in significant improvements in both the number of solved environments (figure 8(a)) and the number of necessary steps (8(b)).

6 System limitations

The main limitation of the system lies in its computational complexity (appendix C), that is caused on one side by the integration of the solver and the action sampling process. While publishing at $\sim 5hz$ proved sufficient for controlling the turtlebot, we reached that frequency by switching to a fixed-step solver and by using a simpler action sampling mechanism, sacrificing precision for speed. While this was possible for the turtlebot experiment, there are many real-world applications where precision and high-frequency control are required. In order to enable the deployment of the proposed method on such systems, two directions in particular seem worth exploring: first, the use of more efficient solvers [41, 42, 43] and second, the possibility of replacing command sampling by a learned policy conditioned on the dynamic model.

7 Conclusion

Motivated by challenges encountered in industrial robotic systems, we proposed ACUMEN, a Model Predictive Control method that handles significant changes in environment dynamics in-between episodes, in settings where most observations and actions are irregular/asynchronous. The solution, which combines meta-learning with neural ODEs, was validated in two simulated environments, the first of which we developed in pybullet[12] based on a real-world industrial robot. The second simulated environment which is tightly associated with ROS was considered in order to evaluate the proposed algorithm in settings close to those of real-world industrial systems. Although those experiments highlight the robustness of ACUMEN to asynchronous/irregular commands and observations as well as its adaptivity to unseen dynamics, its computational complexity —while not prohibitive for the studied examples —remains significant and should be improved in order to make the method applicable to robotic systems requiring high-frequency control.

Acknowledgments

This work was supported by the European Union’s H2020-EU.1.2.2 Research and Innovation Program through FET Project VeriDream under Grant Agreement Number 951992. We wish to thank Quentin Levent for their initial work on the simulation. Likewise, we express our gratitude to Patrick Gallinari and Yuan Yin for their valuable input and criticism during the development of the presented material.

References

- [1] S. Levine, P. Pastor, A. Krizhevsky, J. Ibarz, and D. Quillen. Learning hand-eye coordination for robotic grasping with deep learning and large-scale data collection. *The International journal of robotics research*, 37(4-5):421–436, 2018.
- [2] I. A. OpenAI, M. Andrychowicz, M. Chociej, M. Litwin, B. McGrew, A. Petron, A. Paino, M. Plappert, G. Powell, R. Ribas, et al. Solving rubik’s cube with a robot hand. 2019.
- [3] A. Kumar, Z. Fu, D. Pathak, and J. Malik. Rma: Rapid motor adaptation for legged robots. *arXiv preprint arXiv:2107.04034*, 2021.
- [4] M. Deisenroth and C. E. Rasmussen. Pilco: A model-based and data-efficient approach to policy search. In *Proceedings of the 28th International Conference on machine learning (ICML-11)*, pages 465–472, 2011.
- [5] C. Pinneri, S. Sawant, S. Blaes, J. Achterhold, J. Stueckler, M. Rolinek, and G. Martius. Sample-efficient cross-entropy method for real-time planning. In *Conference on Robot Learning*, pages 1049–1065. PMLR, 2021.
- [6] B. Lim, L. Grillotti, L. Bernasconi, and A. Cully. Dynamics-aware quality-diversity for efficient learning of skill repertoires. In *2022 International Conference on Robotics and Automation (ICRA)*, pages 5360–5366. IEEE, 2022.
- [7] S. Kim, A. Coninx, and S. Doncieux. From exploration to control: learning object manipulation skills through novelty search and local adaptation. *Robotics and Autonomous Systems*, 136:103710, 2021.
- [8] C. Finn, P. Abbeel, and S. Levine. Model-agnostic meta-learning for fast adaptation of deep networks. In *International conference on machine learning*, pages 1126–1135. PMLR, 2017.
- [9] A. Salehi, A. Coninx, and S. Doncieux. Few-shot quality-diversity optimization. *IEEE Robotics and Automation Letters*, 7(2):1–10, 2022.
- [10] C. Yildiz, M. Heinonen, and H. Lähdesmäki. Continuous-time model-based reinforcement learning. In *International Conference on Machine Learning*, pages 12009–12018. PMLR, 2021.
- [11] J. Du, J. Futoma, and F. Doshi-Velez. Model-based reinforcement learning for semi-markov decision processes with neural odes. *Advances in Neural Information Processing Systems*, 33:19805–19816, 2020.
- [12] E. Coumans and Y. Bai. Pybullet, a python module for physics simulation for games, robotics and machine learning. <http://pybullet.org>, 2016–2021.
- [13] Gazebo turtlebot3 simulation. URL <https://emanual.robotis.com/docs/en/platform/turtlebot3/simulation/>.
- [14] Stanford Artificial Intelligence Laboratory et al. Robotic operating system. URL <https://www.ros.org>.
- [15] T. M. Moerland, J. Broekens, and C. M. Jonker. Model-based reinforcement learning: A survey. *arXiv preprint arXiv:2006.16712*, 2020.
- [16] L. Kaiser, M. Babaeizadeh, P. Milos, B. Osinski, R. H. Campbell, K. Czechowski, D. Erhan, C. Finn, P. Kozakowski, S. Levine, et al. Model-based reinforcement learning for atari. *arXiv preprint arXiv:1903.00374*, 2019.
- [17] A. Nagabandi, G. Kahn, R. S. Fearing, and S. Levine. Neural network dynamics for model-based deep reinforcement learning with model-free fine-tuning. In *2018 IEEE International Conference on Robotics and Automation (ICRA)*, pages 7559–7566. IEEE, 2018.
- [18] K. Chua, R. Calandra, R. McAllister, and S. Levine. Deep reinforcement learning in a handful of trials using probabilistic dynamics models. *Advances in neural information processing systems*, 31, 2018.

- [19] R. Rubinstein. The cross-entropy method for combinatorial and continuous optimization. *Methodology and computing in applied probability*, 1(2):127–190, 1999.
- [20] D. Hafner, T. Lillicrap, I. Fischer, R. Villegas, D. Ha, H. Lee, and J. Davidson. Learning latent dynamics for planning from pixels. In *International conference on machine learning*, pages 2555–2565. PMLR, 2019.
- [21] J. Lee and R. S. Sutton. Policy iterations for reinforcement learning problems in continuous time and space—fundamental theory and methods. *Automatica*, 126:109421, 2021.
- [22] M. Abu-Khalaf and F. L. Lewis. Nearly optimal control laws for nonlinear systems with saturating actuators using a neural network hjb approach. *Automatica*, 41(5):779–791, 2005.
- [23] H. Wang, T. Zariphopoulou, and X. Y. Zhou. Reinforcement learning in continuous time and space: A stochastic control approach. *J. Mach. Learn. Res.*, 21(198):1–34, 2020.
- [24] C. Tallec, L. Blier, and Y. Ollivier. Making deep q-learning methods robust to time discretization. In *International Conference on Machine Learning*, pages 6096–6104. PMLR, 2019.
- [25] M. Ghavamzadeh and S. Mahadevan. Continuous-time hierarchical reinforcement learning. In *ICML*, volume 18, pages 186–193, 2001.
- [26] R. T. Chen, Y. Rubanova, J. Bettencourt, and D. K. Duvenaud. Neural ordinary differential equations. *Advances in neural information processing systems*, 31, 2018.
- [27] T. Hospedales, A. Antoniou, P. Micaelli, and A. Storkey. Meta-learning in neural networks: A survey. *IEEE transactions on pattern analysis and machine intelligence*, 44(9):5149–5169, 2021.
- [28] T. Schaul and J. Schmidhuber. Metalearning. *Scholarpedia*, 5(6):4650, 2010. doi:10.4249/scholarpedia.4650. revision #91489.
- [29] Y. Duan, J. Schulman, X. Chen, P. L. Bartlett, I. Sutskever, and P. Abbeel. RL^2 : Fast reinforcement learning via slow reinforcement learning. *arXiv preprint arXiv:1611.02779*, 2016.
- [30] J. Oh, M. Hessel, W. M. Czarnecki, Z. Xu, H. P. van Hasselt, S. Singh, and D. Silver. Discovering reinforcement learning algorithms. *Advances in Neural Information Processing Systems*, 33, 2020.
- [31] Z. Xu, H. P. van Hasselt, and D. Silver. Meta-gradient reinforcement learning. *Advances in neural information processing systems*, 31, 2018.
- [32] O. Vinyals, C. Blundell, T. Lillicrap, D. Wierstra, et al. Matching networks for one shot learning. *Advances in neural information processing systems*, 29:3630–3638, 2016.
- [33] X. Song, W. Gao, Y. Yang, K. Choromanski, A. Pacchiano, and Y. Tang. Es-maml: Simple hessian-free meta learning. *arXiv preprint arXiv:1910.01215*, 2019.
- [34] T. Salimans, J. Ho, X. Chen, S. Sidor, and I. Sutskever. Evolution strategies as a scalable alternative to reinforcement learning. *arXiv preprint arXiv:1703.03864*, 2017.
- [35] P. M. McGuire. *Conveyors: application, selection, and integration*. CRC Press, 2009.
- [36] J. R. Dormand and P. J. Prince. A family of embedded runge-kutta formulae. *Journal of computational and applied mathematics*, 6(1):19–26, 1980.
- [37] N. Koenig and A. Howard. Design and use paradigms for gazebo, an open-source multi-robot simulator. In *2004 IEEE/RSJ International Conference on Intelligent Robots and Systems (IROS)(IEEE Cat. No. 04CH37566)*, volume 3, pages 2149–2154. IEEE, 2004.
- [38] T. Chaffre, J. Moras, A. Chan-Hon-Tong, and J. Marzat. Sim-to-real transfer with incremental environment complexity for reinforcement learning of depth-based robot navigation. *arXiv preprint arXiv:2004.14684*, 2020.
- [39] P. Nikdel, R. Vaughan, and M. Chen. Lbgp: Learning based goal planning for autonomous following in front. In *2021 IEEE International Conference on Robotics and Automation (ICRA)*, pages 3140–3146. IEEE, 2021.
- [40] W. Zhao, J. P. Queralta, and T. Westerlund. Sim-to-real transfer in deep reinforcement learning for robotics: a survey. In *2020 IEEE Symposium Series on Computational Intelligence (SSCI)*, pages 737–744. IEEE, 2020.

- [41] M. Poli, S. Massaroli, A. Yamashita, H. Asama, and J. Park. Hypersolvers: Toward fast continuous-depth models. *Advances in Neural Information Processing Systems*, 33:21105–21117, 2020.
- [42] M. Lehtimäki, L. Paunonen, and M.-L. Linne. Accelerating neural odes using model order reduction. *IEEE Transactions on Neural Networks and Learning Systems*, 2022.
- [43] J. Kelly, J. Bettencourt, M. J. Johnson, and D. K. Duvenaud. Learning differential equations that are easy to solve. *Advances in Neural Information Processing Systems*, 33:4370–4380, 2020.

Appendix A Loss functions

In order to reduce model complexity and improve stability, as is usual in the literature (*e.g.* [4]), we train the dynamic model to predict changes Δz in system state. This process is encapsulated in the function `OptimizeNODE` from algorithm 1. A wide array of choices can be considered for the loss function, but as our aim is to predict pose in all of our experiments, we use the following weighted least squares formulation:

$$\mathcal{L}(\mathcal{T}_j, \theta) = \frac{1}{|\mathcal{D}_{train}|} \sum_{b \in \mathcal{D}_{train}} (E_{trans}^b(\theta) + w_l E_{rot}^b(\theta))^2 \quad (8)$$

where $E_{trans}^b(\theta)$ and $E_{rot}^b(\theta)$ respectively denote the errors in translation and orientation change predictions over example b from the training data, and where $w_l \in \mathbb{R}$ is a weighting coefficient, used values of which are given in table 3. In the presented experiments where displacements are planar, the E_{rot}^b term reduces to an error over the yaw, which in order to avoid discontinuities we simply express as the Frobenius norm of $R_b^T \hat{R}_b$ with R_b, \hat{R}_b respectively the true and predicted rotation matrices.

Appendix B Command selection

As specified throughout the paper, we have not used trainable policies. Instead, actions are sampled and selected based on the state predictions made by the real model. As a result, the proposed method requires a dense reward function that associates a value to each reachable state. The reward functions that we have used for each of our experiments are given in the following subsections, where the particular instantiations of algorithm 2 are also discussed.

B.1 Simulated box rotation

Let us write $d_{trans}^{init} \triangleq \|z_{trans}^{init} - \hat{z}_{trans}\|_2$ the distance between the position predicted by the model and the initial pose of the box on the conveyor belt. Noting $z_{rot}^{target}, \hat{z}_{rot}$ respectively the desired and predicted rotation, the reward for the predicted pose \hat{z} is given by

$$R(\hat{z}) = -\|z_{rot}^{target} - \hat{z}_{rot}\|_2^2 - 10.0\mathbb{I}[d_{trans}^{init} > r_t]d_{trans}^{init} \quad (9)$$

where \mathbb{I} is a predicate function that returns 1.0 if its argument evaluates to true and returns 0.0 otherwise. The threshold r_t was set to 0.3 in our experiments.

The actions sampling mechanism that is used in those experiments results from defining the prior distribution P_ψ of algorithm 2 as a distribution over time-correlated sequences with noise parameter β ([5]). The complete control algorithm is given in algorithm 3.

B.2 Gazebo Turtlebot3 simulation

Keeping the notation for the predicate $\mathbb{I}[\cdot]$ and this time noting $d_{trans}^t \triangleq \|z_{trans}^{target} - \hat{z}_{trans}^t\|_2$ the distance between the position predicted by the model and the target position, we write \hat{z}^t, \hat{z}^{t+1} the predicted poses at timestamps $t, t+1$. In addition to d_{trans} , we consider the difference in angle between the desired heading and the predicted heading:

$$\begin{aligned} v_t &= z_{trans}^{target} - \hat{z}_{trans}^t \\ v_{t+1} &= z_{trans}^{target} - \hat{z}_{trans}^{t+1} \\ u_t^{t+1} &= \cos^{-1}\left(\left(\frac{v_t}{\|v_t\|_2}\right)^T \left(\frac{v_{t+1}}{\|v_{t+1}\|_2}\right)\right) \end{aligned} \quad (10)$$

Algorithm 3: The particular instantiation of algorithm 2 that is used in the simulated box rotation experiments. It results from sampling time-correlated sequences of actions as in [5]. Differences with algorithm 2 have been highlighted in brown. The reward $R(\cdot)$ used in this experiment is given by equation 9.

Input: Neural ODE weights θ , state approximation $\hat{z}(t_0)$ at time t_0 , desired duration of state propagation Δt , previous actions c_1, \dots, c_l (augmented with their timestamp info), **mean and diagonal covariance** μ_0, Σ_0 , population size N_p , number of elites N_e , length of action sequence to sample H , reward function $R(\cdot)$, convergence criterion \mathcal{Y} , **colored noise parameter** β

Output: action sequence a_1^*, \dots, a_H^*

```

1 Function CEMStep( $\theta, \hat{z}(t_0), \{c_1, \dots, c_l\}, \Delta t, \mu_0, \Sigma_0, N_p, N_e, H, R(\cdot), \mathcal{Y}$ ):
2    $\mu = \mu_0$ 
3    $\Sigma = \Sigma_0$ 
4   // initialize elite set
5    $\mathcal{E} = \emptyset$ 
6   while not  $\mathcal{Y}(\Sigma)$  do
7     // sample  $N_p$  action sequences of length  $H$  at regular intervals in  $[t_0, t_0 + \Delta t]$ 
8      $a_{1:H}^1, \dots, a_{1:H}^{N_p} \sim \text{SampleTimeCorrelatedSequence}(\mu, \Sigma, \beta)$ 
9     for each  $a_{1:H}^i$  do
10       $u_i = [c_1, \dots, c_l].\text{concatenate}(a_{1:H}^i)$ 
11      // Let  $\pi_i(t)$  the function that computes actions via interpolating elements of  $u_i$ 
12       $\pi_i = \mathcal{I} \circ u_i$ 
13      // propagate the state
14       $\hat{z}_i = \hat{z}(t_0) + \int_{t_0}^{t_0 + \Delta t} \hat{\mathcal{F}}(\hat{z}(t), \pi_i(t), \theta) dt.$ 
15      // compute associated reward
16       $r_i = R(\hat{z}_i)$ 
17    end
18     $\mathcal{E} = \text{select best } N_e \text{ action sequences according to the } r_i$ 
19     $\mu, \Sigma = \text{fit Gaussian to } \mathcal{E}$ 
20  end
21  // return the best action sequence (alternatively, re-sample using  $\mu, \Sigma$  after convergence)
22  return  $\mathcal{E}$ 

```

Algorithm 4: The action selection mechanism used for the turtlebot can be seen as a particular instance of algorithm 2, which results from setting $H = 1$ and choosing a uniform distribution in the latter. The reward function $R(\cdot)$ which guides actions selection in this set of experiments is defined by equation 11.

Input: Neural ODE weights θ , state approximation $\hat{z}(t_0)$ at time t_0 , desired duration of state propagation Δt , previous actions c_1, \dots, c_l (augmented with their timestamp info), discrete set of actions a_1, \dots, a_l to sample from, number of actions N_p to sample

Output: action sequence a_1^*, \dots, a_H^*

```

1 Function RandomShooting( $\theta, \hat{z}(t_0), \{c_1, \dots, c_l\}, R(\cdot)$ ):
2   // sample  $N_p$  actions to be applied at  $t + \Delta t$ 
3    $a_1, \dots, a_{N_p} \sim \text{SampleUniform}(a_1, \dots, a_l)$ 
4   for each  $a_i$  do
5      $u_i = [c_1, \dots, c_l].\text{concatenate}(a_i)$ 
6     // Let  $\pi_i(t)$  the function that computes actions via interpolating elements of  $u_i$ 
7      $\pi_i = \mathcal{I} \circ u_i$ 
8     // propagate the state
9      $\hat{z}_i = \hat{z}(t_0) + \int_{t_0}^{t_0 + \Delta t} \hat{\mathcal{F}}(\hat{z}(t), \pi_i(t), \theta) dt.$ 
10    // compute associated reward
11     $r_i = R(\hat{z}_i)$ 
12  end
13   $a_{best} = \text{select best action according to the } r_i$ 
14  return  $a_{best}$ 

```

and define the reward as

$$R(\hat{z}_{t+1}) = -d_{trans} - \mathbb{I}[u_t^{t+1} > r_t^{t+1}]u_t^{t+1}. \quad (11)$$

In other words, the error on the heading is ignored when it falls below the threshold r_t^{t+1} , which was fixed to 5° in our experiments.

In contrast with the simulated box rotation experiments, we found that the turtlebot required more frequent changes in controls which could be achieved by setting $\beta = 0$ (that is equivalent to sampling according to a Gaussian prior). Furthermore, we found that setting $H = 1$ and sampling from a discrete set of velocity values was sufficient to solve the navigation task. A natural additional benefit of this simpler sampling (algorithm 4) is the reduced computation time required to return a decision.

Appendix C Computation time.

We used a standard desktop computer equipped with an AMD Ryzen Threadripper 1920X 12-Core Processor for benchmarking.

Simulated Box rotation. On average, a single integration of the neural ODE with a batch size of 20 took $210ms$ while a single forward of the RNN with the same batch size took $3ms$. Similarly, training the neural ODE over a single batch of size 5 took an average of $380ms$ versus an average of $61ms$ for the recurrent model. Note that the high cost of training and inference with neural ODEs was in part due to the choice of an adaptive-step solver (dopri-5). Furthermore, the sampling-based control used in these experiments (appendix B) added some overhead, resulting in decision frequencies of respectively $\sim 10Hz$ and $\sim 1Hz$ for the neural ODEs.

Real-time simulated Turtlebot3 control. a single forward pass of the RNN with batch size 21, took on average $4ms$, while the integration for the same batch using the ODE solver (RK4 in this case) took on average $82ms$. In other terms, neural ODEs took about $20\times$ more time to produce a decision. Similarly, an epoch of training on 120 samples took an average of $2.63s$ for neural ODEs and an average of $0.9s$ for RNNs. Those results are hardly surprising as vanilla neural ODEs are notoriously slow [41].

That being said, as in this particular application, using neural ODEs can actually lead to lower overall computational costs for higher P_{drop} values. For example, for $P_{drop} = 0.5$, the increased length and irregularity of the trajectories produced by the RNNs resulted in execution times that exceeded $35min$ for some episodes, while the maximum length reached for neural ODE based episode was $7.1min$. This is coherent with figure 7(d).

Appendix D Algorithm hyperparameters

In all experiments, the dynamic model \hat{F} of equation 4.1 was approximated using feed-forward neural networks with \tanh activations, taking as input at each integration time-step t the vector $(t, \pi(t), \hat{z}_t)^T$ concatenating the time, interpolated command and the propagated state. For the simulated box rotation experiments, four hidden layers, each of dimension 48 were used. For the gazebo turtlebot3 simulation, five hidden layers of dimensions $[64, 128, 128, 64, 64]$ were used. The stacked RNNs used in each section had approximately the same capacity as the neural ODEs they were compared to. While the neural ODE used in the simulated conveyor belts experiments had $8k$ parameters, the corresponding stacked RNN had 5 hidden layers of dimension 32, resulting in about $9k$ parameters. Similarly, the neural ODE used to control the turtlebot had $37k$ parameters and we used a stacked RNN with 5 hidden layers of dimension 64 to match this number of parameters.

	N	r_{split}	α	σ	N_{it}	$\tau_i.timeout$	$train_{freq}$	ODE solver	N-ODE learning rate	γ_{decay}	w_l
Simulated box rotation	20	0.75	5e-4	1e-2	10	300	5	dopri5	5e-4	0.9	10.0
Gazebo Turtlebot3 simulation	25	0.75	5e-5	5e-3	1	640	40	RK4	1e-4	0.99	1.0

Table 3: Training hyper-parameters for both the outer and lower level optimization problems.

For the simulated box rotation experiments, the CEM-based action selection method (algorithm 3) with hyper-parameters $N_p = 20, N_e = 5, \mu_0 = \mathbf{0}, \Sigma_0 = I, H = 4, \beta = 2$ was used. In the case of the turtlebot, we found that sampling commands with no time correlation ($\beta = 0$) allowed for quicker recovery from wrong command selections. Furthermore, while the model was pretrained on continuous commands sampled from a uniform distribution over $[-0.22, 0.22]$, as mentioned in the previous section (appendix §B, algorithm 4), we found that choosing the actions from a limited discretized set produced satisfactory results during con-

trol: in the presented control experiments, linear and angular velocity control were respectively chosen from $\{-0.1, -0.05, -0.01, 0.0, 0.01, 0.05, 0.1\}$ and $\{-0.1, 0.0, 0.1\}$.

The hyperparameters for the meta update (line 30 in algorithm 1) as well as the hyper-parameters for the training of the neural ODEs are reported in table 3.